International Journal of Thin Films Science and Technology

http://dx.doi.org/10.18576/ijtfst/120105

Visible Light-Assisted Degradation of Malachite Green dye using Waste Tea-Mediated Zinc Nanoparticles

Rehana Baiju Mampilly[1], *Amanullakhan Pathan*[2,*] *and C. P. Bhasin*[1]

[1]Department of Chemistry, Hemchandracharya North Gujarat University, Patan-384265, India
[2]Shri Sarvajanik Science College (PG), Mehsana-384001, India

Received: 2 Aug. 2022, Revised: 4 Sep. 2022, Accepted: 4 Oct. 2022
Published online: 1 Jan. 2023

Abstract: This work presents entirely a new, green, and non-expensive route of synthesis of zinc nanoparticles (NPs) using waste tea. The crystalline nature of waste tea-mediated Zn NPs (WT-ZnO NPs) was confirmed by XRD and SAED analyses. Further characterizations of WT-ZnO NPs were done using UV-vis spectroscopy, FTIR spectroscopy, SEM-EDX, and TEM. The size of synthesized NPs was calculated to be 15.1 nm which presented spherical morphology with some sorts of agglomeration. The WT-ZnO NPs when applied as visible light-driven photo catalyst for degradation of Malachite green dye. Adsorptions of Malachite green (MG) dye follow pseudo-first-order kinetics. It was found that the dye degradation showed best results in the presence of sunlight at a pH of 3, Malachite green (MG) Dye concentration 50 ppm with 60 mg of WT-ZnO NPs. At room temperature, the maximum removal of dye was achieved in 105 min by stirring. Malachite green (MG) showed that degradation was 96.45 % in the presence of visible light and 81.5% in the presence of sun light within the experimental time. The highly pure, WT-ZnO NPs are considered to have comparable photocatalytic activity with respect to most of the reported works and hence might find a way for its practical application for waste water treatment in the real world. The WT-ZnO NPs could be reused at least for three times without any significant loss in degradation efficiency.

Keywords: Waste tea, photocatalytic degradation, WT-ZnO NPs, malachite green dye.

1 Introduction

Nanotechnology primarily concerns the study of particles ranging from 1 to 100 nm in size. An interdisciplinary field, Nanotechnology incorporates bio nanoscience, materials science, and technology [1], and relies heavily on the fields of biology, chemistry, and physics. Nanoparticles are widely used in a range of applications owing to their optical, biological, and physiochemical properties [2-5]. Nanoparticles can be synthesized using physical, chemical, and biological methods [6,7]. Biological nanoparticle synthesis typical involves the use of microorganisms, fungi, algae, and plants. The green synthesis method has recently become widely used, as it allows the use of less toxic chemicals [8] that are safe when released into the environment. Green-synthesized nanoparticles produced from plants are also more stable. Nanoparticles have a wider range of applications relative to larger particles as they have a much higher surface area to volume ratio, which allows them to act as active components more efficiently [9]. Metal oxides typically form closely packed structures and often exhibit antimicrobial, magnetic, and catalytic qualities [10]. Green-synthesized nanoparticles are highly compatible, and so they can be used in several biomedical and pharmaceutical applications [11]. ZnO NPs are widely used in the packaging of food and in the production of paints and varnishes [12]. They also block harmful UV radiation, a quality which makes them valuable in the production of cosmetics and sunscreens [6].

Metal oxide nanoparticles possess catalytic qualities and as such are commonly used in the elimination of toxic hazardous chemical substances, primarily in the field of environmental safety [13]. The catalytic properties of ZnO NPs are due to their crystal structure, porosity, surface area, size distribution, and band gap, and are often used in photocatalytic degradation [14]. Recently, number studies are reported on photocatalytic capacity of ZnO NPs [15-18]. Due to its high photostability, non-toxicity, thermal stability, oxidation resistivity, high electron mobility, biocompatibility, biodegenerability, broad absorption range, and wide band gap (~3.37 eV), ZnO is an important inorganic semiconductor material. It has been employed widely in diverse applications such as solar cells, biosensors, gas sensors, detectors, photonic devices, optoelectronic devices, cosmetics, drug delivery, nanomedicines, and as an efficient, cost-effective

*Corresponding author E-mail: amankhan255@gmail.com

alternative to TiO_2 in photocatalysis [19-30]. ZnO NPs possess numerous active sites, and thus they have a high reaction rate to allow the effective generation of hydrogen peroxide, which makes them suitable for the photocatalytic removal of organic pollutants from water bodies. The effluents produced by textile, leather, cosmetics, paper, printing, plastic, rubber, and pharmaceutical industries usually contain synthetic dyes and their metabolites, which are toxic, carcinogenic, mutagenic, stable to light and oxidizing agents, and non-biodegradable in nature [31-32]. Toxicity analyses of industrial effluents have been performed extensively using different bioassays [33-35]. The waste waters produced by dyeing industries have the highest level of toxicity, with cytotoxic, genotoxic, and mutagenic effects [36-42]. Thus, it is essential to remove dye pollutants from industrial effluents before they reach natural water bodies. Moreover, bio-toxicity evaluations have indicated remarkable reductions in the toxicity of the reaction products/metabolites formed after the photodegradation of dyes [37].

Biological synthesis of nanoparticles using plant extracts is becoming an emerging area of research in nano-biotechnology due to its simplicity, low cost, nontoxicity and environmentally friendly nature. Moreover, nanoparticles are produced by plant extracts are more stable and biocompatible in comparison with those produced by physical/chemical methods. Based on the literature, biosynthesis of ZnO NPs were reported by using plant extracts including *Aloe vera* [43] (leaf), *Nephelium lappaceum L* [44] (fruit peel), *Corymbia citriodora* [45] (leaf), *Polygala tenuifolia* [46] (root), *Trifolium pratense* [47] (flower), *Rosa canina* [48] (fruit), *Zingiber officinale* [49] (rhizome), *Eucalyptus globulus* [50] (leaf) and *Vitex trifolia L*. [51] (leaf).

In the present study, we demonstrate a green and eco-friendly route for the synthesis of ZnO NPs using aqueous extract of Waste Tea. X-ray diffraction (XRD), energy dispersive X-ray spectroscopy (EDX), field emission scanning electron microscope (FESEM), transmission electron microscopy (HR-TEM) and Fourier transform infrared spectroscopy (FTIR) was used for characterizing the Waste Tea mediated ZnO (WT-ZnO) NPs. The photocatalyst activity of WT-ZnO NPs was also investigated using malachite green (MG) dye as the model pollutant under visible and solar light irradiation

2 Experimental

2.1 Materials

All the reagents are of analytical grade and were used without any further purification. Zinc nitrate hexahydrate ($Zn(NO_3)_2.6H_2O$) was purchased from *s.d.* fine chemicals while MG was purchased from Hi- media. Waste tea (Wagh Bakri) was collected from the tea shop in market. Deionized water was used throughout the experimental study. Glass wares were thoroughly cleaned and dried inside an oven at 100^0C for 2 h before use. A hot plate with magnetic stirrer and a centrifuge machine of model Remi were used for heating and centrifuging purpose of the work.

2.2 Preparation of Waste tea extract (WTE):

Young shoots of purple tea as collected were chopped into fine pieces using a kitchen knife. These were then air dried for about 2 h. Then 80 g of the chopped pieces of the shoots were heated in 500 ml deionized water at 80◦ C for 90 min until purplish color of the mixture appeared. Finally, the mixture was cooled, centrifuged, and filtered through Watmann filter paper No. 1 twice to get the extract which was then stored at −4◦C for further use.

2.3 Green Synthesis of WT-ZnO nanoparticles

The tea extracts (black and green) were prepared by adding 60g tea into 1000ml distilled water and heating them at 353 K for 60 min in a water bath and the extract were vacuum filtered. After cooling to the room temperature, then 0.10 mol/L $Zn(NO_3)_2$ solutions was added to the tea extracts with a ratio volume of 1:2. The Zn nanoparticles were formed when black Zn NPs were observed in the solution mixed Zn (II) and tea extracts. The resulting solution was centrifuged for 15 min; the supernatant was discarded and the pellets were washed 3 times with distilled water to remove unreacted salts and tea phytochemicals on the colloidal surface. Following a final wash, the iron particles were centrifuged, the supernatant was discarded and particles were dried in an oven.

2.4 Characterization of WT-ZnO NPs

Synthesized WT-ZnO nanoparticles were characterized by following various analytical techniques. Fourier transform infrared (FTIR) spectra of synthesized zinc nanoparticles were recorded on a Shimadzu instrument in the range of 4000–400 cm-1 using KBr pellet technique. X-ray powder diffraction (XRD) analysis was carried out on a Rigaku D/max 40 kV diffractometer equipped with the graphite mono chromator and Cu target, from our department. Field emission gun scanning electron microscope (FEG-SEM) images were recorded on a JSM-7600F series instrument and High-resolution transmission electron microscope (HR-TEM) images were recorded on a Tecnai G2-F30 electron microscope, from SICART VallabhVidhyanagar. The sample preparation was carried out via the coating on carbon coated grid Cu Mesh 300 prior to the measurement. The adsorption properties of iron nanoparticles were recorded by UV–1800, Shimadzu spectrophotometer.

2.5 Photocatalytic performance

The photocatalytic performance of WT-ZnO NPs has been investigated by the degradation organic dye Malachite Green (MG). All the photocatalytic experiments were carried out at room temperature under illumination of visible light using 100W tungsten lamp and sunlight. Dyes used were of concentration 50 ppm and the catalyst dosage was 60 mg. Firstly MG (50 ml) were separately degraded using the 60 mg catalyst dose. All the solutions containing photo catalyst were sonicated for 1 min for complete dispersion prior to illumination by visible light. The photo degradation process was monitored using UV-Vis spectrophotometer at the maximum absorbance of the respective dyes, MG (λmax ~ 617 nm)) in their solution at a time interval of 15 min for a contact time of 105 min. The degradation efficiency (η) and rate constant (k) for the photocatalytic reaction has been calculated using the Equations (1) and (2) given below.

$$\textit{Degradation}\ (\%) = \frac{C_0 - C}{C_0} \times 100 \ldots\ldots\ldots\ldots (1)$$

$$ln\left(\frac{C_0}{C_t}\right) = kt \ldots\ldots\ldots\ldots\ldots\ldots (2)$$

Here C_0 and C_t represent the initial and final absorbance of the dyes at λ_{max} and k is the first-order rate constant (sec^{-1}). The similar degradation experiments of single and mixed dyes were monitored in dark in presence and in absence of photo catalyst. Of course, degradation experiments were also monitored using visible light and sunlight.

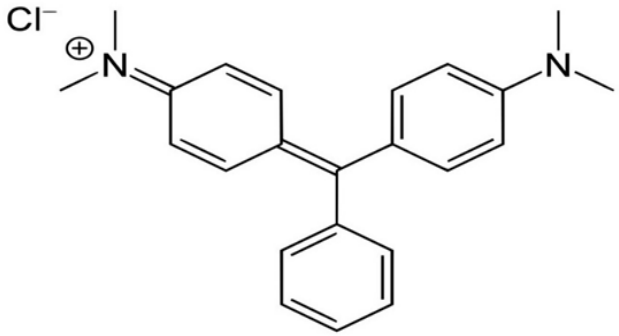

Fig. 1: Structure of Malachite Green Dye.

3 Result and Discussion

3.1 Characterization of iron nanoparticles

3.1.1 FTIR spectra ZnO nanoparticles

Exhibit 2 represents the FTIR spectrum of WT-ZnO NPs which evidenced the involvement of Phyto compounds of purple tea in the synthesis. Various bands arising from FTIR spectrum are 3408, 1401, 1031, 856, 696, and 441 cm^{-1}. The band between 450 and 600 cm^{-1} is pronounced for ZnO bending vibration while sharp band at ~ 441 cm^{-1} confirmed Zn-O stretching vibration [52,53]. The broad band at ~ 3408 cm^{-1} shows the existence of H-bonded phenolic groups which is confirmed by the presence of a band due to C-O stretching vibration at ~1031 cm^{-1}. The band at ~ 401 cm^{-1} may be assigned to C=C stretching vibration of aromatic rings. Lastly the sharp but weak band appearing at ~ 856 and 696 cm^{-1} may be assigned to the out of plane C-H bending vibration. These peaks are hence found to be enriched with moieties of Phyto compounds of purple tea and played the prime role in the synthesis of WT-ZnO NPs. The data obtained from FTIR analysis supports the UV-Vis analysis and hence confirms the formation of WT-ZnO NPs.

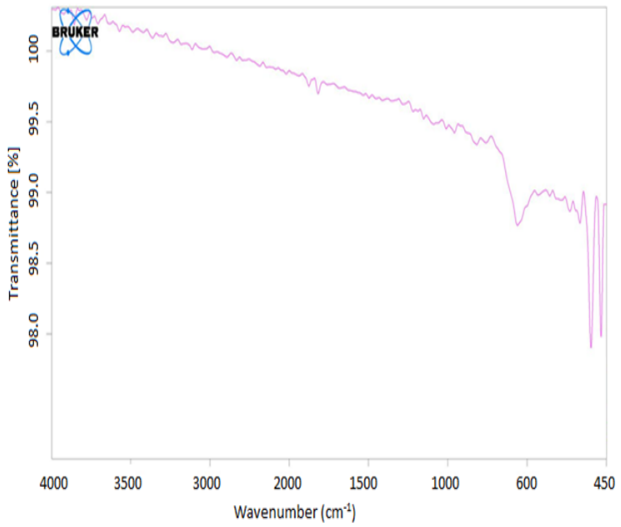

Fig. 2: FTIR spectra of WT-ZnO NPs.

3.1.2 X-ray diffraction spectra of WT-ZnO NPs:

The XRD pattern of Phyto synthesized WT-ZnO NPs (Exhibit 3) was taken to examine the crystalline nature of the sample. The distinctive diffraction peak at 2θ = 31.8, 34.5, 36.3, 47.8, 56.7, 62.9, 66.5, 67.9, 69.2, 72.9, and 77.0 are assigned to (100), (002), (101), (102), (110), (103), (200), (112), (201), (004), and (202) crystal planes, respectively. All the diffraction peaks are well indexed to hexagonal phase (wurtzite structure) which had an excellent match with reported JCPDS File No. 89–0511. Moreover, the diffraction pattern showed in the figure presenting sharp peaks with well-defined intensity proves the presence of crystalline form of WT-ZnO NPs.

3.1.3 Field emission gun scanning electron microscope (FEG-SEM) WT-ZnO NPs:

SEM image of WT-ZnO NPs [Exhibit-4(a)] presented nearly spherical and uniformly distributed NPs with some sorts of agglomeration. The agglomeration among the

WT-ZnO NPs might be due to the capping effect of phenolic compounds [54].

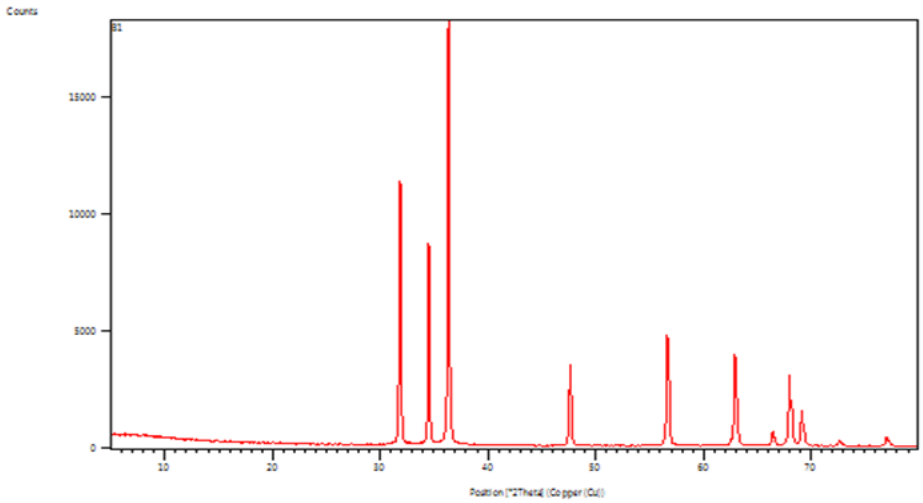

Fig.3: XRD spectra of WT-ZnO NPs.

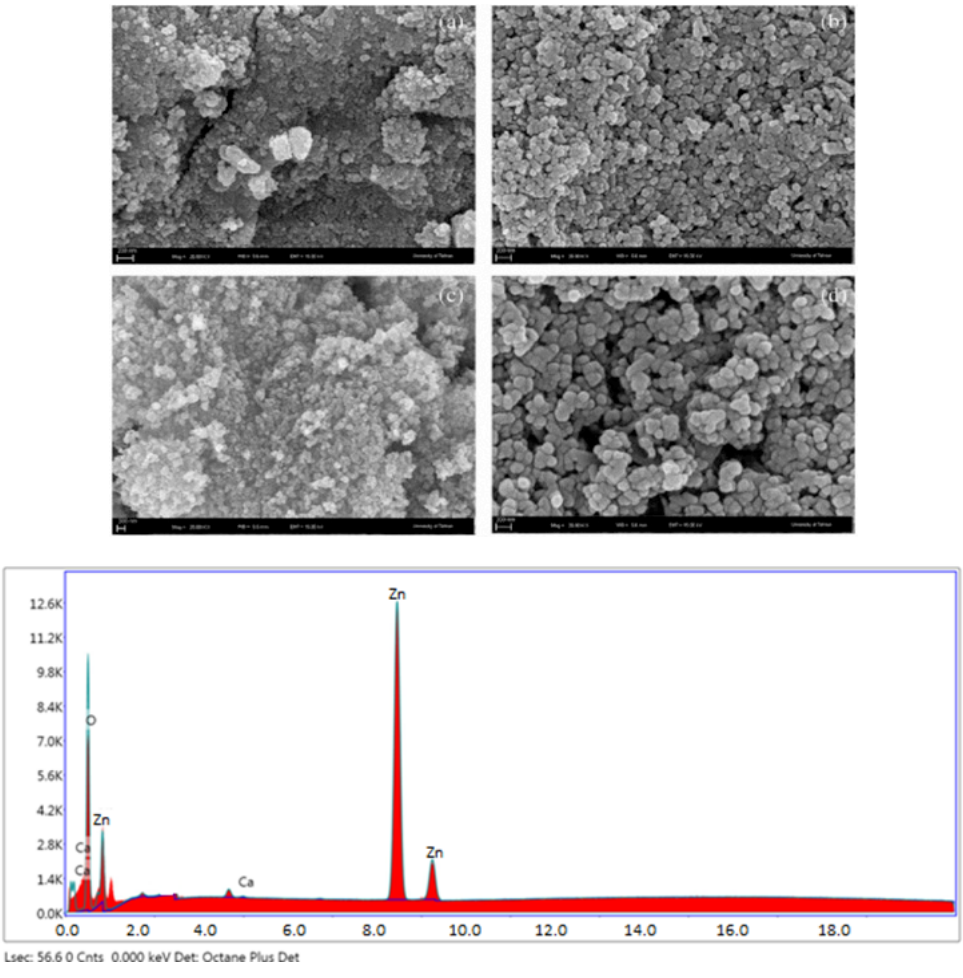

Fig.4: FE-SEM (a) with EDAX (b) spectra of WT-ZnO Nanoparticles.

The elemental information of WT-ZnO NPs depicted in the EDX spectrum [(Exhibit 4(b)] shows the presence of highest peak at 1, 8.6, and 9.6 keV for Zn and 0.5 keV for O. As no other peaks related to any other impurity are detected in the spectrum confirms the high purity of WT-ZnO NPs. The green synthesized WT-ZnO NPs have weight % of 81.24 of Zn and 18.05 of O. Moreover, the atomic percentage of Zn and O are 51.56 and 48.04, respectively. Such findings are assumed to be advanced to published reports where the presence of Zn and O in ZnO NPs is accompanied by the presence of other impurities.

3.1.4 High resolution transmission electron microscope (HR-TEM) of WT-ZnO NPs:

The HR-TEM images of WT-ZnO NPs presented in Exhibit 5 (a) and (b) reflected the appearance of mostly spherical in addition to few hexagonal shaped particles which are slightly agglomerated. The size of as synthesized WT-ZnO NPs ranged from 5 to 30 nm which is displayed from the histogram distribution of particle size [Exhibit-5(a)]. It can also be noticed from the [Exhibit 5(b)] that most of the particles fall in the range of 10–20 nm and the average mean size of the particle came out to be 15.1 nm.

3.2 Various Parameters Which Effects on Malachite Green (MG) Dye adsorption in the presence of WT-ZnO Nanoparticles

3.2.1 Effect of Nanoparticles dosage

Waste Tea mediated WT-ZnO nanoparticles utilized is likely to alter the dye degradation process, different amounts of nanoparticles were used. **Table-1** summaries the findings. When the amount of adsorbent dose was increased, the percentage of Malachite Green (MG) elimination likewise rose. This is due to the increased Zinc surface area and more accessible adsorption active site, however after adding a particular amount (60 mg) of an adsorbent, the rate became practically constant. This could be because, beyond a certain point, increasing the amount of adsorbent did not increase the adsorbent's exposed surface area (active sites). As the adsorbent covered the bottom of the reaction tank, it only increased the thickness of the layer. It is possible that a saturation point was reached, and that after this saturation point, no effect of adsorbent quantity was detected.

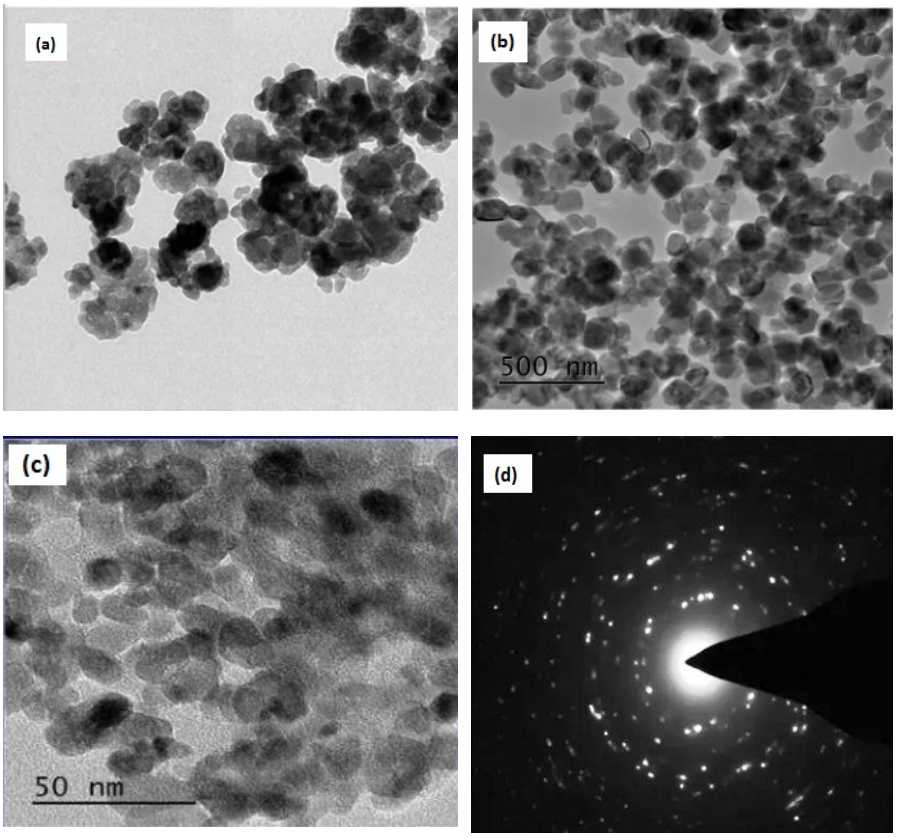

Fig.5: HR-TEM images of WT-ZnO Nanoparticles.

Table 1: Effect of adsorbent dosage on the adsorption of Malachite Green (MG) by WT-ZnO nanoparticles.

Amount of adsorbent (mg)	% of removal of MG dye in presence of WT-ZnO nanoparticles	
	With sun light	With visible light
10	55.60	68.20
20	62.70	74.02
30	68.60	82.45
40	76.10	88.30
50	80.25	93.45
60	86.80	96.55
70	85.65	95.51
80	84.30	95.53

Malachite Green (MG)dye =50ppm, pH=6.5, Temperature=29±1

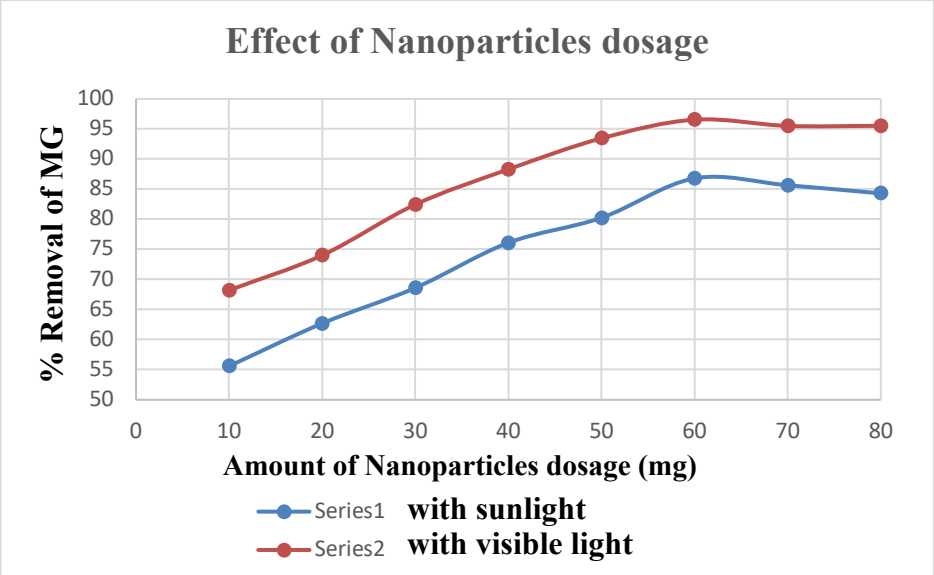

Fig.6: Effect of adsorbent dosage on the adsorption of Malachite Green (MG) by WT-ZnO nanoparticles.

This theory was also supported using reaction containers of various sizes. As the bottom area of the vessel increased, so did the adsorbent exposed area, and thus the percentage of dye removal increased. In the current study, beakers of the same size were used for the whole experiment, and after a maximum exposure to adsorbent, additional adsorbent addition simply raised the layer thickness, but did not of adsorbent was successful in achieving the greatest removal percentage in Malachite Green (MG) dye.

3.2.2 Effect of pH

Because the charge of a surface on adsorbent and dye molecules can be modified by pH values in aqueous

solution, the initial pH value is one of the most important elements influencing the removal process of dyes for water

Table 2: Effect of pH on the adsorption of Malachite Green (MG) by iron nanoparticles.

pH	% of removal of Malachite Green (MG) dye in presence of iron nanoparticles	
	With sun light	With visible light
3.0	64.30	71.20
3.5	65.95	78.35
4.0	69.45	83.65
4.5	73.70	87.76
5.0	75.40	89.05
5.5	79.74	90.66
6.0	82.80	93.90
6.5	85.30	96.20
7.0	84.82	95.80
7.5	83.20	94.65
8.0	83.40	94.80

Malachite Green (MG)dye =50ppm, Dosage= 60 mg, Temperature=29±1ºc

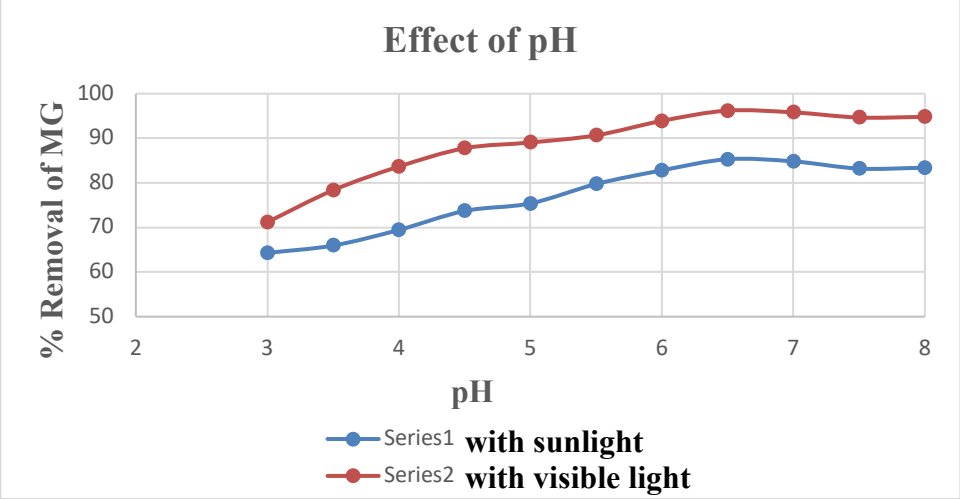

Fig. 7: Effect of pH on the adsorption of Malachite Green (MG)by WT-ZnO nanoparticle.

treatment. Table 2 investigates the influence of dye solution pH on adsorption. The experiments were carried out at a fixed adsorbate concentration (60 ppm), adsorbent dosage of 0.60 g, and a temperature of 29±1ºC. The pH was altered by adding 0.1M HCl or 0.1M NaOH, and the dye's adsorption was tested throughout a pH range of 3.0-8.0. Malachite Green (MG) is a cationic dye that exists in aqueous solution as positively charged ions. As a charged ion, the degree of its adsorption onto the surface of WT-ZnO NPs is mostly affected by the adsorbent's surface charge, which is influenced by the solution pH.

Figure 7 depicts the obtained results, which show that adsorption of Malachite Green (MG) increases with increasing pH from 3.0 to 6.5, and that when pH increases further, the percent of removal of Malachite Green (MG) begins to decrease. This is because the surface activities of Zn NPs change from positive to negative charge when pH increases, resulting in electrostatic interaction between the adsorbent and Malachite Green (MG) molecules. As seen in Figure 7, as the pH rises from 3 to 6.5, the proportion of dye removed rises, and as the pH rises from 6.5 to 8, the percentage of dye removed falls. At pH 6.5, WT-ZnO nanoparticles absorbed the most Malachite Green (MG). The maximal degradation of Malachite Green (MG) dye with Zn NPs was approximately 96.20 % in the presence of visible light and 85.3 % in the presence of sunlight respectively.

3.2.3 Effect of concentration

The initial concentration of Malachite Green (MG) was varied from 50 ppm to 250 ppm. The results are reported in Table 3.

It has been discovered that as the initial Malachite Green (MG) concentration increases from 50 ppm to 250 ppm, the equilibrium adsorption increases. The findings are due to the fact that when the initial concentration increases, the mass transfer driving force increases, resulting in greater Malachite Green (MG) adsorption. It was also discovered that the percentage of dye removed decreases as the original concentration of Malachite Green (MG) dye increases. According to Figure 8, the greatest dye removal by waste tea mediated WT-ZnO NPs was 96.40 % (in presence of visible light) and 85.63 % (in presence of Sun light) in a 50-ppm solution of Malachite Green (MG) dye.

3.2.4 Effect of Contact Time

The most essential parameter in adsorption dye removal is the influence of contact time. All of the experiments were carried out over a set period of time. Table 4 shows the association between dye removal effectiveness of the Malachite Green (MG) dye and contact time. It is apparent that the percentage of dye removal increases as contact duration increases. The effects of contact time on the removal of Malachite Green (MG) dye were investigated in a set time interval. Figure-9 depicts the influence of contact time on the removal of Malachite Green (MG) dye by adsorbent.

Table 3: Effect of concentration on the adsorption of Malachite Green (MG) by WT-ZnO nanoparticles.

Dye concentration (ppm)	% of removal of Malachite Green (MG) dye in presence of WT-ZnO nanoparticles	
	With sun light	With visible light
50	85.63	96.40
100	78.65	90.78
150	73.15	86.54
200	72.25	83.60
250	70.85	80.20

Nanoparticles Dosage= 60 mg, pH= 6.5, Temperature=29±1ºC

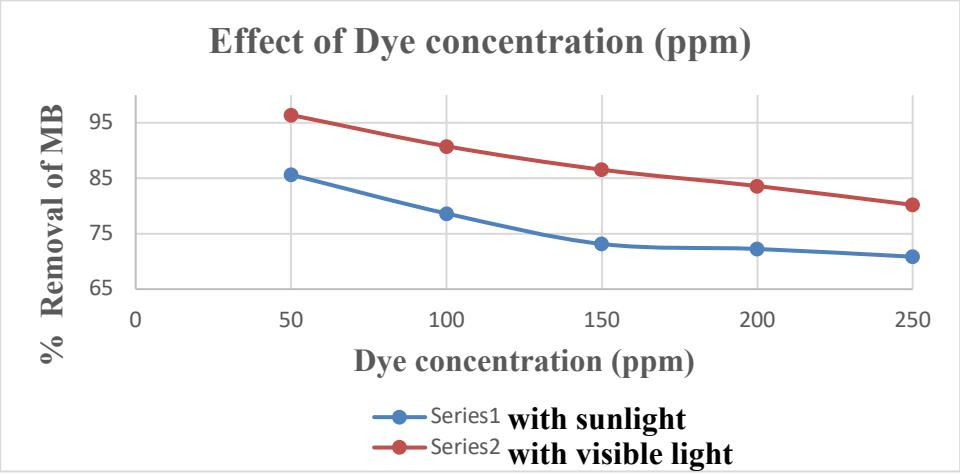

Fig. 8: Effect of concentration on the adsorption of Malachite Green (MG) by WT-ZnO Nanoparticles.

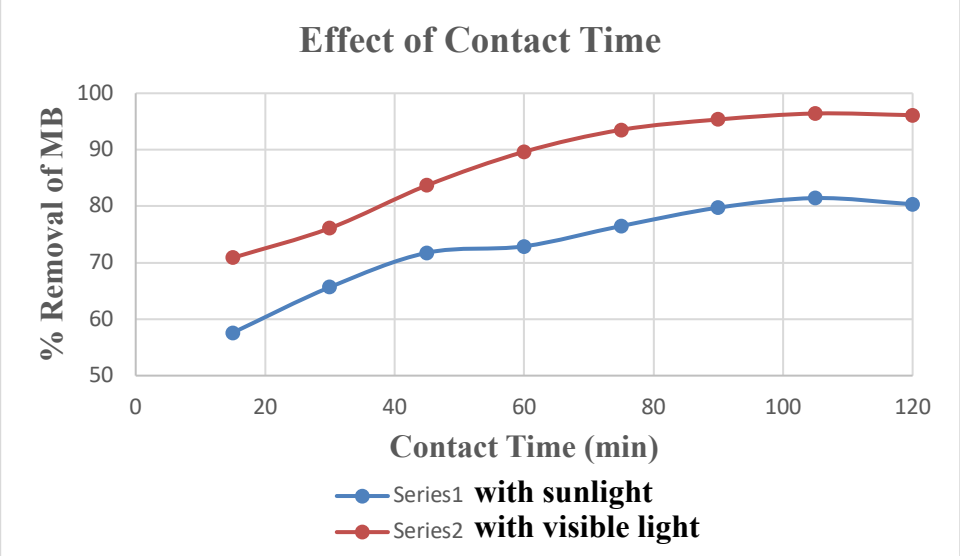

Fig. 9: Effect of contact time on the removal of MG by WT-ZnO nanoparticles.

Table 4: Effect of contact time on the removal of Malachite Green (MG) by WT-ZnO nanoparticles.

Contact Time (min)	% of removal of Malachite Green (MG) dye in presence of WT-ZnO nanoparticles	
	With sun light	With visible light
0	0.00	0.00
15	57.60	70.87
30	65.67	76.12
45	71.76	83.70
60	78.90	89.64
75	71.50	93.53
90	79.75	95.36
105	81.44	96.42
120	80.35	96.12

Malachite Green (MG) dye =50ppm, Dosage= 60 mg, pH=6.5, Temperature = 29±1

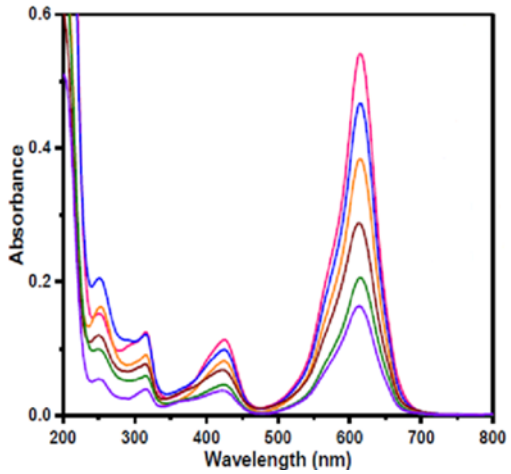

Fig. 10: UV-Vis absorption spectra for degradation of Malachite Green (MG)dye in the presence of WT-ZnO Nanoparticles.

The availability of a significant number of unoccupied sites for Malachite Green (MG) adsorption can be attributed to the rapid adsorption at initial contact time, but the slow rate of dye adsorption could be related to slow pore diffusion of the dye into the bulk adsorbent. Maximum dye removal was achieved at 105 minutes utilizing WT-ZnO NPs, which was approximately 96.42 % in the presence of visible light and 81.5% in the presence of sun light.

3.2.5 Possible mechanism of dye degradation

$$ZnO + h\gamma \longrightarrow ZnO\ (e_{CB}^{-} + h_{VB}^{+})$$

$$ZnO\ (h_{VB}^{+}) + {}^{-}OH \longrightarrow {}^{\cdot}OH + ZnO$$

$$ZnO\ (e_{CB}^{-}) + O_2 \longrightarrow O_2 + ZnO$$

$$2\ {}^{\cdot}O_2 + 2H_2O \longrightarrow 2\ {}^{\cdot}HO_2 + H_2O_2$$

$$H_2O_2 \longrightarrow 2\ {}^{\cdot}OH$$

WT- ZnO can absorb Visible light and generate electron–hole pairs. Based on the obtained results and previous reports one can suggest that the electron produced from the surface of catalyst react with surface adsorbed O_2 to form $O_2^{\bullet}$. The positively charged WT-ZnO surface and/or the $^{\bullet}O_2$ can react with surface adsorbed H_2O to form $^{\bullet}OH$, however, the later step is mostly responsible for generation of $^{\bullet}OH$ radical. The $^{\bullet}OH$ is a potent in discriminant oxidizing agent which possibly responsible for degradation of most of the surface adsorbed dye molecules. To further assess the roles of $^{\bullet}OH$ active species, tertiary butanol (TBA) (1.0 mM) was used as scavenger to quench the hydroxyl active species during the degradation of dye molecules. As shown in Fig. 10, the photocatalytic degradation of MG over the WT-ZnO was significantly affected after the addition of TBA, indicating that $^{\bullet}OH$ active species played a significant role in the photocatalytic degradation of dyes.

3.3 Comparison of photo catalytic degradation of EBT in presence of various Photocatalysts and light sources.

Photocatalyst	Dyes	Dye conc. and vol.	Light source	Catalyst load	Time (min)	Degradation %	References
ZnO	MG	10 ppm, 50 ml	Sunlight	50 mg	180	99	(Aminuzzaman [55] *et al.,* 2018)
ZnO	RB	10 μM, 100 ml	Sunlight	20 mg	200	98	(Varadavenkatesan [56] *et al.,* 2019)
ZnO	RB	9.5 ppm, 50 ml	UV	100 mg	50	100	(Prasad [57] *et al.,* 2019)
ZnO	MG	10 ppm, 10 ml	UV	2 mg	120	89.5	(Rajapriya [58] *et al.,* 2020)
PT-ZnO	MG	10 ppm, 50 ml	Visible	50 mg	90	89	(Das [59] *et al.,* 2021)
PT-ZnO	RB	10 ppm, 50 ml	Visible	50 mg	90	22	(Das [59] *et al.,* 2021)
WT-ZnO	MG	50 ppm	Visible	60 mg	105	96.3	Present work

4 Conclusions

In summary, the current investigation demonstrates a facile greener method for the synthesis of WT-ZnO using the waste tea extract as structure directing agent. The newly synthesized WT-ZnO was investigated for the photocatalytic degradation of MG dye degradation using visible light and sunlight as light source. WT-ZnO exhibits hexagonal wurtzite structure with an average particle size of 15 nm were confirmed by HR-TEM and XRD analysis. The chemical purity/composition and elemental state of WT-ZnO were confirmed by EDS analysis. The vibrational modes of FTIR such as the bending and stretching properties have also confirmed the formation of WT-ZnO. The WT-ZnO exhibited degradation efficiency of MG dyes approximately 96.42 % in the presence of visible light and 81.5% in the presence of sun light. MG dye degraded within 105 min of contact time. It was found that the dye degradation showed best results in the presence of sunlight at a pH of 3, Malachite green (MG) Dye concentration 50 ppm with 60 mg of WT-ZnO NPs.

References

[1] Divya, M., Vaseeharan, B., Abinaya, M., Vijayakumar, S., Govindarajan, M., Alharbi, N. S., ... & Benelli, G. (2018). Biopolymer gelatin-coated zinc oxide nanoparticles showed high antibacterial, antibiofilm and anti-angiogenic activity. Journal of Photochemistry and Photobiology B: Biology, 178, 211-218.

[2] Ramesh, P., Rajendran, A., & Meenakshisundaram, M. (2014). Green syntheis of zinc oxide nanoparticles using flower extract cassia auriculata. Journal of NanoScience and NanoTechnology, 2(1), 41-45.

[3] Karthika, V., Arumugam, A., Gopinath, K., Kaleeswarran, P., Govindarajan, M., Alharbi, N. S., ... & Benelli, G. (2017). Guazuma ulmifolia bark-synthesized Ag, Au and Ag/Au alloy nanoparticles: Photocatalytic potential, DNA/protein interactions, anticancer activity and toxicity against 14 species of microbial pathogens. Journal of Photochemistry and Photobiology B: Biology, 167, 189-199.

[4] Benelli, G., Maggi, F., Pavela, R., Murugan, K., Govindarajan, M., Vaseeharan, B., ... & Higuchi, A. (2018). Mosquito control with green nanopesticides: towards the One Health approach? A review of non-target effects. Environmental Science and Pollution Research, 25(11), 10184-10206.

[5] Nagajyothi, P. C., Sreekanth, T. V. M., Tettey, C. O., Jun, Y. I., & Mook, S. H. (2014). Characterization, antibacterial, antioxidant, and cytotoxic activities of ZnO nanoparticles using Coptidis Rhizoma. Bioorganic & medicinal chemistry letters, 24(17), 4298-4303.

[6] Vijayakumar, S., Vaseeharan, B., Malaikozhundan, B., & Shobiya, M. (2016). Laurus nobilis leaf extract mediated green synthesis of ZnO nanoparticles: characterization and biomedical applications. Biomedicine & Pharmacotherapy, 84, 1213-1222.

[7] Ishwarya, R., Vaseeharan, B., Kalyani, S., Banumathi, B., Govindarajan, M., Alharbi, N. S., ... & Benelli, G. (2018). Facile green synthesis of zinc oxide nanoparticles using Ulva lactuca seaweed extract and evaluation of their photocatalytic, antibiofilm and insecticidal activity. Journal of Photochemistry and Photobiology B: Biology, 178, 249-258.

[8] Singh, T., Jyoti, K., Patnaik, A., Singh, A., Chauhan, R., & Chandel, S. S. (2017). Biosynthesis, characterization and antibacterial activity of silver nanoparticles using an endophytic fungal supernatant of Raphanus sativus. Journal of Genetic Engineering and Biotechnology, 15(1), 31-39.

[9] Alivov, Y. I., Kalinina, E. V., Cherenkov, A. E., Look, D. C., Ataev, B. M., Omaev, A. K., ... & Bagnall, D. M. (2003). Fabrication and characterization of n-ZnO/p-AlGaN heterojunction light-emitting diodes on 6H-SiC substrates. Applied Physics Letters, 83(23), 4719-4721.

[10] Vijayakumar, S., Mahadevan, S., Arulmozhi, P., Sriram, S., & Praseetha, P. K. (2018). Green synthesis of zinc oxide nanoparticles using Atalantia monophylla leaf extracts: Characterization and antimicrobial analysis. Materials Science in Semiconductor Processing, 82, 39-45.

[11] Kumar, B., Smita, K., Cumbal, L., & Debut, A. (2014). Green approach for fabrication and applications of zinc oxide nanoparticles. Bioinorganic chemistry and applications, 2014.

[12] Jamdagni, P., Khatri, P., & Rana, J. S. (2018). Green synthesis of zinc oxide nanoparticles using flower extract of Nyctanthes arbor-tristis and their antifungal activity. Journal of King Saud University-Science, 30(2), 168-175.

[13] Santhoshkumar, J., Kumar, S. V., & Rajeshkumar, S. (2017). Synthesis of zinc oxide nanoparticles using plant leaf extract against urinary tract infection pathogen. Resource-Efficient Technologies, 3(4), 459-465.

[14] Fowsiya, J., Madhumitha, G., Al-Dhabi, N. A., & Arasu, M. V. (2016). Photocatalytic degradation of Congo red using Carissa edulis extract capped zinc oxide nanoparticles. Journal of Photochemistry and Photobiology B: Biology, 162, 395-401.

[15] Atchudan, R., Edison, T. N. J. I., Perumal, S., Karthikeyan, D., & Lee, Y. R. (2016). Facile synthesis of zinc oxide nanoparticles decorated graphene oxide composite via simple solvothermal route and their photocatalytic activity on methylene blue degradation. Journal of Photochemistry and Photobiology B: Biology, 162, 500-510.

[16] Atchudan, R., Edison, T. N. J. I., Perumal, S., Karthik, N., Karthikeyan, D., Shanmugam, M., & Lee, Y. R. (2018). Concurrent synthesis of nitrogen-doped carbon dots for cell imaging and ZnO@ nitrogen-doped carbon sheets for photocatalytic degradation of methylene blue. Journal of Photochemistry and Photobiology A: Chemistry, 350, 75-85.

[17] Muthuchamy, N., Atchudan, R., Edison, T. N. J. I., Perumal, S., & Lee, Y. R. (2018). High-performance glucose biosensor based on green synthesized zinc oxide nanoparticle embedded nitrogen-doped carbon sheet. Journal of Electroanalytical chemistry, 816, 195-204.

[18] Atchudan, R., Edison, T. N. J. I., Perumal, S., Shanmugam, M., & Lee, Y. R. (2017). Direct solvothermal synthesis of zinc oxide nanoparticle decorated graphene oxide nanocomposite for efficient photodegradation of azo-dyes.

Journal of Photochemistry and Photobiology A: Chemistry, 337, 100-111.

[19] Matinise, N., Fuku, X. G., Kaviyarasu, K., Mayedwa, N., & Maaza, M. J. A. S. S. (2017). ZnO nanoparticles via Moringa oleifera green synthesis: Physical properties & mechanism of formation. Applied Surface Science, 406, 339-347.

[20] Özgür, Ü., Alivov, Y. I., Liu, C., Teke, A., Reshchikov, M., Doğan, S., ... & Morkoç, A. H. (2005). A comprehensive review of ZnO materials and devices. Journal of applied physics, 98(4), 11.

[21] Ludi, B., & Niederberger, M. (2013). Zinc oxide nanoparticles: chemical mechanisms and classical and non-classical crystallization. Dalton Transactions, 42(35), 12554-12568.

[22] Prasad, A. R., Ammal, P. R., & Joseph, A. (2018). Effective photocatalytic removal of different dye stuffs using green synthesized zinc oxide nanogranules. Materials Research Bulletin, 102, 116-121.

[23] Kołodziejczak-Radzimska, A., & Jesionowski, T. (2014). Zinc oxide—from synthesis to application: a review. Materials, 7(4), 2833-2881.

[24] Wang, Z. L. (2004). Zinc oxide nanostructures: growth, properties and applications. Journal of physics: condensed matter, 16(25), R829.

[25] Hernández-Alonso, M. D., Fresno, F., Suárez, S., & Coronado, J. M. (2009). Development of alternative photocatalysts to TiO 2: challenges and opportunities. Energy & Environmental Science, 2(12), 1231-1257.

[26] Tian, C., Zhang, Q., Wu, A., Jiang, M., Liang, Z., Jiang, B., & Fu, H. (2012). Cost-effective large-scale synthesis of ZnO photocatalyst with excellent performance for dye photodegradation. Chemical Communications, 48(23), 2858-2860.

[27] Premanathan, M., Karthikeyan, K., Jeyasubramanian, K., & Manivannan, G. (2011). Selective toxicity of ZnO nanoparticles toward Gram-positive bacteria and cancer cells by apoptosis through lipid peroxidation. Nanomedicine: Nanotechnology, Biology and Medicine, 7(2), 184-192.

[28] Xiong, H. M. (2013). ZnO nanoparticles applied to bioimaging and drug delivery. Advanced Materials, 25(37), 5329-5335.

[29] Malaikozhundan, B., Vaseeharan, B., Vijayakumar, S., Pandiselvi, K., Kalanjiam, M. A. R., Murugan, K., & Benelli, G. (2017). Biological therapeutics of Pongamia pinnata coated zinc oxide nanoparticles against clinically important pathogenic bacteria, fungi and MCF-7 breast cancer cells. Microbial pathogenesis, 104, 268-277.

[30] Vijayakumar, S., Vaseeharan, B., Malaikozhundan, B., & Shobiya, M. (2016). Laurus nobilis leaf extract mediated green synthesis of ZnO nanoparticles: characterization and biomedical applications. Biomedicine & Pharmacotherapy, 84, 1213-1222.

[31] Rathnasamy, R., Thangasamy, P., Thangamuthu, R., Sampath, S., & Alagan, V. (2017). Green synthesis of ZnO nanoparticles using Carica papaya leaf extracts for photocatalytic and photovoltaic applications. Journal of Materials Science: Materials in Electronics, 28(14), 10374-10381.

[32] Prasad, A. R., & Joseph, A. (2017). Synthesis, characterization and investigation of methyl orange dye removal from aqueous solutions using waterborne poly vinyl pyrrolidone (PVP) stabilized poly aniline (PANI) core–shell nanoparticles. RSC advances, 7(34), 20960-20968.

[33] Iqbal, M. (2016). Vicia faba bioassay for environmental toxicity monitoring: a review. Chemosphere, 144, 785-802.

[34] Noreen, M., Shahid, M., Iqbal, M., & Nisar, J. (2017). Measurement of cytotoxicity and heavy metal load in drains water receiving textile effluents and drinking water in vicinity of drains. Measurement, 109, 88-99.

[35] Iqbal, M., Abbas, M., Arshad, M., Hussain, T., Ullah Khan, A., Masood, N., ... & Ahmad Khera, R. (2015). Short Communication Gamma Radiation Treatment for Reducing Cytotoxicity and Mutagenicity in Industrial Wastewater. Polish Journal of Environmental Studies, 24(6).

[36] Abbas, M., Adil, M., Ehtisham-ul-Haque, S., Munir, B., Yameen, M., Ghaffar, A., ... & Iqbal, M. (2018). Vibrio fischeri bioluminescence inhibition assay for ecotoxicity assessment: a review. Science of the Total Environment, 626, 1295-1309.

[37] Iqbal, M., & Nisar, J. (2015). Cytotoxicity and mutagenicity evaluation of gamma radiation and hydrogen peroxide treated textile effluents using bioassays. Journal of Environmental Chemical Engineering, 3(3), 1912-1917.

[38] Iqbal, M., Abbas, M., Nisar, J., Nazir, A., & Qamar, A. (2019). Bioassays based on higher plants as excellent dosimeters for ecotoxicity monitoring: a review. Chemistry International, 5(1), 1-80.

[39] Pathan, A. A., Desai, K. R., & Bhasin, C. P. (2017). Improved photocatalytic properties of NiS nanocomposites prepared by displacement method for removal of rose bengal dye. Current Nanomaterials, 2(3), 169-176.

[40] Pathan, A. A., Prajapati, C. G., Dave, R.P. & Bhasin, C. P. (2022). Effective and Feasible Photocatalytic Degradation of Janus Green B dye in Aqueous Media using PbS/CTAB Nanocomposites. Int. J. Thin. Fil. Sci. Tec. 11(2), 245-255.

[41] Desai, K. R., Pathan, A. A., & Bhasin, C. P. (2017). Synthesis, characterization of cadmium sulphide nanoparticles and its application as photocatalytic degradation of congored. International Journal of Nanomaterials and Chemistry, 3(2), 39-43.

[42] Pathan, A. A., Bhatt, S. H., Vajapara, S.J. & Bhasin, C. P. (2022). Solar Light Induced Photo Catalytic Properties of α-Fe_2O_3 Nanoparticles for Degradation of Methylene Blue Dye. Int. J. Thin. Fil. Sci. Tec. 11(2), 213-224.

[43] Ali, K., Dwivedi, S., Azam, A., Saquib, Q., Al-Said, M. S., Alkhedhairy, A. A., & Musarrat, J. (2016). Aloe vera extract functionalized zinc oxide nanoparticles as nanoantibiotics against multi-drug resistant clinical bacterial isolates. Journal of colloid and interface science, 472, 145-156.

[44] Karnan, T., & Selvakumar, S. A. S. (2016). Biosynthesis of

ZnO nanoparticles using rambutan (Nephelium lappaceumL.) peel extract and their photocatalytic activity on methyl orange dye. Journal of molecular Structure, 1125, 358-365.

[45] Zheng, Y., Fu, L., Han, F., Wang, A., & Cai, W. (2015). Yu J et al. Green Chem. Lett. Rev., 2015, 8.

[46] Nagajyothi, P. C., Cha, S. J., Yang, I. J., Sreekanth, T. V. M., Kim, K. J., & Shin, H. M. (2015). Antioxidant and anti-inflammatory activities of zinc oxide nanoparticles synthesized using Polygala tenuifolia root extract. Journal of Photochemistry and Photobiology B: Biology, 146, 10-17.

[47] Dobrucka, R., & Długaszewska, J. (2016). Biosynthesis and antibacterial activity of ZnO nanoparticles using Trifolium pratense flower extract. Saudi journal of biological sciences, 23(4), 517-523.

[48] Jafarirad, S., Mehrabi, M., Divband, B., & Kosari-Nasab, M. (2016). Biofabrication of zinc oxide nanoparticles using fruit extract of Rosa canina and their toxic potential against bacteria: a mechanistic approach. Materials Science and Engineering: C, 59, 296-302.

[49] Anbuvannan, M., Ramesh, M., Viruthagiri, G., Shanmugam, N., & Kannadasan, N. (2015). Synthesis, characterization and photocatalytic activity of ZnO nanoparticles prepared by biological method. Spectrochimica Acta Part A: Molecular and Biomolecular Spectroscopy, 143, 304-308.

[50] Siripireddy, B., & Mandal, B. K. (2017). Facile green synthesis of zinc oxide nanoparticles by Eucalyptus globulus and their photocatalytic and antioxidant activity. Advanced Powder Technology, 28(3), 785-797.

[51] Elumalai, K., Velmurugan, S., Ravi, S., Kathiravan, V., & Raj, G. A. (2015). Bio-approach: Plant mediated synthesis of ZnO nanoparticles and their catalytic reduction of methylene blue and antimicrobial activity. Advanced Powder Technology, 26(6), 1639-1651.

[52] Pai, S., Sridevi, H., Varadavenkatesan, T., Vinayagam, R., & Selvaraj, R. (2019). Photocatalytic zinc oxide nanoparticles synthesis using Peltophorum pterocarpum leaf extract and their characterization. Optik, 185, 248-255.

[53] Mehr, E. S., Sorbiun, M., Ramazani, A., & Fardood, S. T. (2018). Plantmediated synthesis of zinc oxide and copper oxide nanoparticles by using Ferulago angulata (schlecht) boiss extract and comparison of their pho- to catalytic degradation of Rhodamine B (RhB) under visible light irradiation. Journal of Materials Science: Materials in Electronics, 29, 1333–1340.

[54] Dhanemozhi, A. C., Rajeswari, V., & Sathyajothi, S. (2017). Green synthesis of zinc oxide nanoparticle using green tea leaf extract for supercapacitor application. Materials Today: Proceedings, 4(2), 660-667.

[55] Aminuzzaman, M., Ying, L. P., Goh, W. S., & Watanabe, A. (2018). Green synthesis of zinc oxide nanoparticles using aqueous extract of Garcinia mangostana fruit pericarp and their photocatalytic activity. Bulletin of Materials Science, 41(2), 1-10.

[56] Varadavenkatesan, T., Lyubchik, E., Pai, S., Pugazhendhi, A., Vinayagam, R., & Selvaraj, R. (2019). Photocatalytic degradation of Rhodamine B by zinc oxide nanoparticles synthesized using the leaf extract of Cyanometra ramiflora. Journal of Photochemistry and Photobiology B: Biology, 199, 111621.

[57] Prasad, A. R., Garvasis, J., Oruvil, S. K., & Joseph, A. (2019). Bioinspired green synthesis of zinc oxide nanoparticles using Abelmoschus esculentus mucilage and selective degradation of cationic dye pollutants. Journal of Physics and Chemistry of Solids, 127, 265–274.

[58] Rajapriya, M., Sharmili, S. A., Baskar, R., Balaji, R., Alharbi, N. S., Kadaikunnan, S., ... & Vaseeharan, B. (2020). Synthesis and characterization of zinc oxide nanoparticles using Cynara scolymus leaves: Enhanced hemolytic, antimicrobial, antiproliferative, and photocatalytic activity. Journal of Cluster Science, 31(4), 791-801.

[59] Das, J., Das, K. C., Thakurata, D. G., & Dhar, S. S. (2021). Visible light assisted degradation of binary mixture of dyes using purple tea mediated zinc oxide nanoparticles. Environmental Quality Management, 1−9.